Drought Identification and Prediction from GNSS Time Series Using SSA and Hybrid CNN-Transformer

Motahareh Esfandyari Kaloukan[1], Shirin Malihi[2 *], Siavash Iran-Pour[3], Danesh Shokri[4], Saeid Homayouni[5]

[1] Department of Geomatics Engineering, University of Isfahan, Iran - mt.esfandyari@gmail.com
[2] Civil Engineering Department, University of Cambridge, United Kingdom - sm2852@cam.ac.uk
[3] Department of Geomatics Engineering, University of Isfahan, Iran - iranpour.siavash@gmail.com
[4] Département des Sciences Géomatiques, Université Laval, Canada - danesh.shokri.1@ulaval.ca
[5] Centre Eau Terre Environnement, Institut National de la Recherche Scientifique, Canada - saeid.homayouni@inrs.ca

Keywords: Drought, Climate monitoring, GNSS time series, Singular Spectrum Analysis, CNN-Transformer

Abstract

In recent decades, global climate change has triggered a rise in extreme environmental phenomena, including prolonged droughts, intensified precipitation events, and shifts in tidal patterns. This study focuses on the application of the observations from Global Navigation Satellite System (GNSS) signals for monitoring and classifying climatic conditions, with particular emphasis on drought. Using daily vertical displacement data from a GNSS station in California (2005–2023), we developed a robust analysis framework. It includes data cleaning (removing outliers, filling gaps, detecting offsets, and modeling noise), trend and seasonal pattern extraction through Singular Spectrum Analysis (SSA), feature generation (like amplitude, energy, and dominant frequency), labeling based on the Standardized Precipitation-Evapotranspiration Index (SPEI), and classification using a hybrid CNN-Transformer model. The results demonstrate the model’s capability to accurately detect drought periods (SPEI $<$ -1) characterized by diminished amplitudes in seasonal components and heightened noisy fluctuations, as well as wet periods (SPEI $>$ 1) marked by elevated energy in semi-annual signals. The model was evaluated with an overall accuracy of 83.3 percent, an F1-score of 0.90 for the drought class, and successful classification of newly observed data (2024–2025) and scenario-based extrapolation for 2026–2029. This approach, independent of traditional meteorological data, underscores the potential of GNSS as a geodetic tool for environmental monitoring, albeit with limitations such as reliance on single stations and the need for supplementary datasets. The methodology holds promise for enhancing early warning systems and climate models. At the time of model development (2023), the period 2024–2029 was treated as future data and used to assess the extrapolation capability of the proposed model. While real observations for 2024–2025 later became available, the remaining years represent a scenario-based forecast derived from learned temporal patterns rather than operational meteorological prediction.

1. Introduction

In recent decades, the Earth’s climate system has undergone significant and accelerating changes, manifesting itself in the form of extreme and sometimes unpredictable natural phenomena. Events such as prolonged droughts, intense rainfall, and shifts in tidal patterns are increasingly attributed to global climate variability. While traditionally considered separate from climate processes, even geophysical events like earthquakes have been explored in terms of their potential links to environmental stress and melting of glaciers in tectonically active regions [1]. These changes not only threaten ecosystems and human settlements but also challenge the scientific community to develop more accurate monitoring, modeling, and forecasting systems. Understanding these phenomena and their interconnections is critical for developing sustainable responses to an evolving climate [2].

The GNSS is composed of three main segments: the space segment, which includes a constellation of orbiting satellites; the control segment, responsible for monitoring and maintaining satellite operations; and the user segment, which consists of receivers that collect signals transmitted by the satellites. These signals are used to determine precise positioning and timing information on Earth’s surface [3]. One of the key outputs of GNSS is a time series of positional data collected from ground-based permanent stations. These data, typically expressed in daily or sub-daily displacements in three dimensions (north, east, and vertical), can reveal subtle ground movements over time. Such displacement records are not only essential for studying tectonic activities but also for identifying climate-related changes. For instance, seasonal surface deformations caused by hydrological loading, glacial melting, or permafrost thawing can be detected by analysing these GNSS-derived time series. The ability of GNSS to provide continuous, high-precision geodetic measurements makes it a valuable tool in the detection and quantification of environmental processes associated with climate change [4].

Over the past two decades, a growing body of research has leveraged geodetic tools, particularly GNSS, to investigate climate-related surface deformation and environmental change[5]. For example, Blewitt et al. [6] demonstrated how continuous GNSS networks can detect vertical ground movements associated with groundwater variations. van Dam et al. [7] investigated atmospheric pressure and hydrological loading effects on GNSS coordinates. Tregoning and Watson [8] analysed sea-level changes using vertical land motion derived from GNSS. Dong et al. [9] linked GNSS time series with seasonal snow loading. Herring et al. [5] applied GNSS data to estimate elastic deformation from hydrological processes. Argus et al. [10] focused on the mass loss from the Greenland and Antarc-

* **Corresponding author**

tic ice sheets using GNSS vertical motion. Furthermore, Fu and Freymueller [11] demonstrated the sensitivity of GNSS to seasonal freezing and thawing of the permafrost. These studies underscore the value of GNSS as a climate-sensitive tool capable of capturing short- and long-term responses of the Earth's surface to environmental forcing.

Despite significant advancements in observational techniques and data processing methods, several challenges remain in accurately monitoring and analysing climate change impacts. One of the main difficulties is the integration of multi-source data with varying temporal and spatial resolutions, such as GNSS, satellite imagery, and in-situ measurements. Differences in data quality, availability, and processing standards often complicate large-scale assessments. Additionally, distinguishing climate-induced deformation signals from other geophysical or anthropogenic sources (e.g., tectonics, groundwater extraction, urbanization) requires sophisticated filtering and modelling techniques. Another major challenge is the scarcity of long-term, high-quality geodetic data in remote or developing regions, which limits our ability to perform global-scale analyses. Furthermore, while tools like GNSS and InSAR are powerful, they require advanced technical expertise and computational resources, posing barriers for widespread adoption in climate monitoring. These challenges highlight the need for more integrated, accessible, and automated analytical frameworks that can reliably extract climate signals from complex and noisy geospatial datasets.

It is important to emphasize that GNSS-derived vertical deformation is strongly site-dependent and influenced by local geological structure, groundwater extraction, soil properties, land cover, and anthropogenic activities. Therefore, the present study does not claim universal drought predictability, but rather investigates the feasibility of GNSS-based drought classification within a specific hydro-climatic context.

Global Navigation Satellite System (GNSS) stations provide millimeter-level position measurements that are not only essential for geodetic and tectonic applications but also highly sensitive to surface mass loading variations. Among the three position components, the vertical displacement is particularly responsive to hydrological changes. Both uplift and subsidence can occur during droughts. While reduced surface loading may cause uplift in the short term, prolonged droughts and groundwater extraction can lead to subsidence. Therefore, vertical GNSS displacements are considered a general indicator of hydrological fluctuations. Therefore, the vertical GNSS time series serve as an indirect but powerful proxy for monitoring hydrological extremes such as droughts and wet periods. By linking GNSS-derived vertical displacements with drought indices such as the Standardized Precipitation Evapotranspiration Index (SPEI), it becomes possible to translate geodetic observations into hydrological insights and classify years into drought, normal, and wet conditions.

In this study, we utilize daily GNSS position time series data, focusing on the vertical component, as a novel source of information to monitor hydro-climatic conditions. While GNSS has traditionally been applied for geophysical studies such as tectonic deformation or seismic monitoring, its sensitivity to surface mass loading makes it a promising proxy for detecting climate-related signals. The objective of this work is to identify characteristic frequencies associated with drought and wet conditions directly from GNSS time series. To achieve this, we propose a deep learning-based framework that integrates Convolutional Neural Networks (CNN) for feature extraction and Transformer architectures for capturing long-term temporal dependencies (see Figure 1). The classification scheme is designed as a three-class problem, distinguishing between drought, normal, and wet conditions. Our approach demonstrates that GNSS-derived position time series, when combined with advanced deep learning models, can provide an effective and independent tool for climate variability monitoring.

2. Data Collection

In this study, daily GNSS position time series from station P242, referenced to the IGS14 frame, were analyzed. The dataset spans January 2007 to January 2025 and includes three-dimensional coordinates (North, East, and Vertical). The station is located in Santa Cruz County, California, USA (36.95°N, 121.46°W; Figure 2), a region characterized by recurrent drought and pronounced hydro-climatic variability, making it suitable for investigating deformation signals associated with terrestrial water storage changes.

The analysis focuses on the vertical displacement component due to its sensitivity to elastic surface deformation induced by hydrological mass loading, including precipitation variability and groundwater storage fluctuations. The time series were preprocessed to remove outliers and temporal gaps and subsequently normalized prior to feature extraction. Figure 3 presents the vertical displacement record of station P242, where time (years) is shown on the horizontal axis and displacement (mm) on the vertical axis. The series exhibits clear seasonal oscillations, a gradual long-term subsidence trend, and several offsets likely associated with equipment maintenance or localized environmental influences.

The use of a single GNSS station was intended to establish a methodological proof-of-concept under controlled hydro-climatic conditions. Although this design limits spatial generalization, it enables a clearer evaluation of the relationship between vertical deformation signals and drought indicators. Future work will extend the framework to multi-station networks to assess spatial transferability.

3. Methodology

This section outlines the methodological framework developed to extract climatic frequency components and classify drought conditions using GNSS vertical time series data. The end-to-end analytical pipeline, illustrated in Figure 1, is structured into five major phases: (1) preprocessing, including gap filling, offset detection, noise modeling, and component decomposition using Singular Spectrum Analysis (SSA) into trend, annual, and semi-annual signals; (2) frequency decomposition to isolate climatic components; (3) feature engineering from decomposed signals; (4) climatic condition labeling based on external drought indices; and (5) deep learning-based classification using a hybrid CNN-Transformer architecture.

3.1 GNSS Time Series Preprocessing

The raw GNSS vertical displacement time series obtained from station P242 spans multiple years and includes inherent complexities such as instrument changes, environmental effects, and

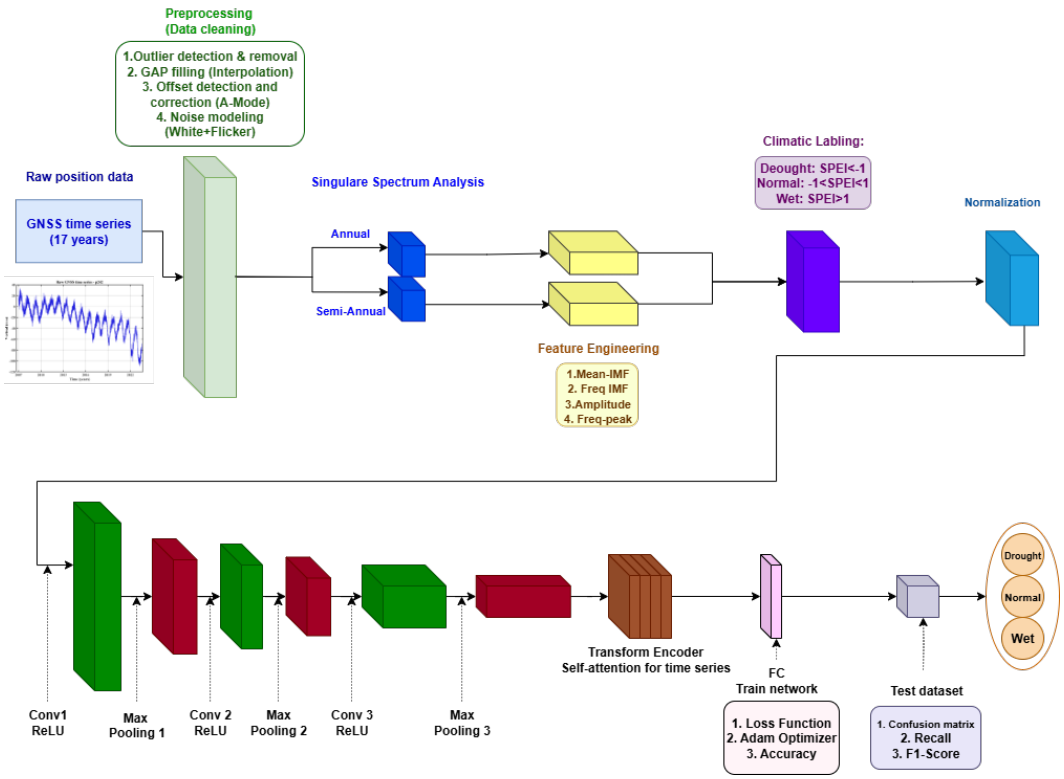

Figure 1. End-to-end workflow for classifying hydrological conditions (Drought/Normal/Wet) from GNSS vertical displacement at station P242. The pipeline performs outlier removal, gap filling, offset detection/correction, and noise modeling, followed by time–frequency decomposition and feature extraction. The extracted features are then fed into a CNN–Transformer classifier to assign each year to Drought, Normal, or Wet.

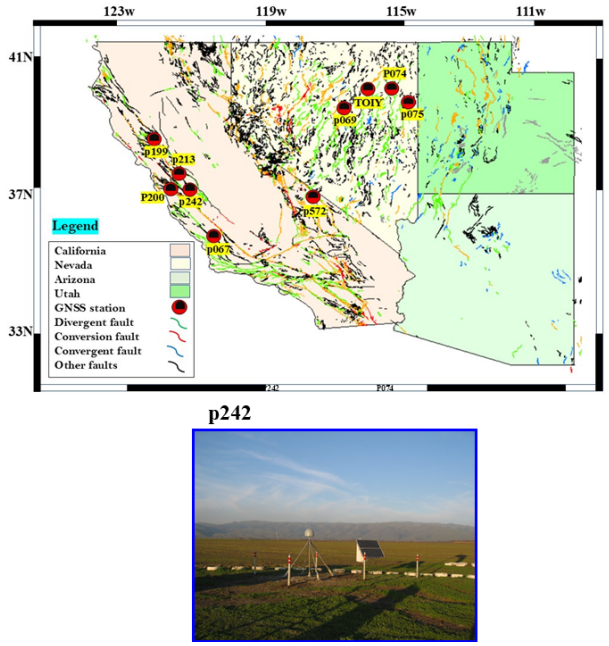

Figure 2. Study area in California (top) and location of GNSS station P242 (bottom).

noise. To prepare the data for reliable frequency decomposition and deep learning classification, a comprehensive preprocessing pipeline was applied. This stage aims to remove non-climatic artifacts, normalize the data range, and ensure continuity and consistency.

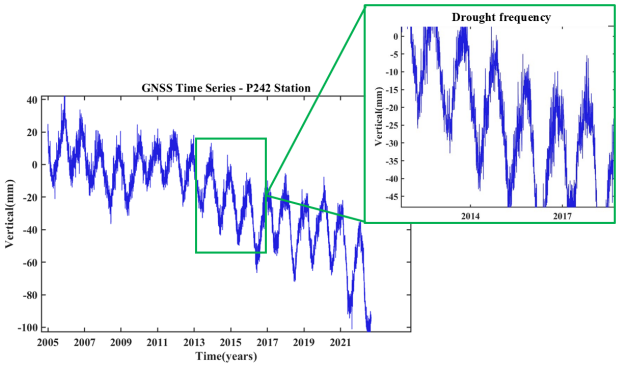

Figure 3. Illustration of drought frequency in GNSS time series at P242 station.

Prior to analysis, the GNSS vertical displacement time series underwent several preprocessing steps to ensure data quality and reliability. First, outliers, often caused by hardware glitches, atmospheric disturbances, or satellite errors, were detected using Z-score filtering. Observations exceeding ± 3 standard deviations from a moving average were flagged and excluded [12, 13].

Second, to address short-term data gaps, linear interpolation was applied. For a gap between time steps t_1 and t_2 with known values $y(t_1)$ and $y(t_2)$, the interpolated value at $t \in (t_1, t_2)$ was computed as:

$$y(t) = y(t_1) + \frac{t - t_1}{t_2 - t_1} [y(t_2) - y(t_1)] \quad (1)$$

This method preserves long-term trends while avoiding artificial oscillations [14, 15]. Third, discontinuities in the time series, typically introduced by equipment changes, maintenance, or possible tectonic events, were identified and corrected using the Amplitude Mode (A-Mode) method. A design matrix A was constructed containing candidate offset locations, and the generalized least squares solution was estimated as:

$$\hat{x} = (A^\top Q^{-1} A)^{-1} A^\top Q^{-1} v \tag{2}$$

where v is the residual vector after detrending, A is the offset design matrix (with 1s at possible offset times), Q is the noise covariance matrix (white + flicker noise model), and $\hat{x}$ represents the estimated offset magnitudes. The significance of each offset was then tested using a chi-squared test:

$$\Delta v = v - A\hat{x}, \quad \chi^2 = \Delta v^\top Q^{-1} \Delta v \tag{3}$$

with offsets retained if

$$\chi^2 > \chi^2_{1-\alpha,\, df}, \quad \alpha = 0.02,\ df = 1 \tag{4}$$

Finally, the stochastic characteristics of the GNSS time series were modeled using a composite noise framework combining white and flicker noise. The total power spectral density $S(f)$ was expressed as:

$$S(f) = \sigma_w^2 + \frac{\sigma_f^2}{f} \tag{5}$$

where σ_w^2 is the white noise variance, σ_f^2 is the flicker noise strength, and f is frequency. This comprehensive preprocessing framework ensures that the GNSS time series is free from spurious artifacts, properly corrected for offsets, and statistically characterized for subsequent frequency-domain and deep learning analyses. It should be noted that the GNSS time series were obtained from standard geodetic processing solutions (IGS14 frame), in which tropospheric delays are estimated and removed as part of the parameter adjustment process. Therefore, residual tropospheric effects are expected to be minimal.

3.2 Singular Spectrum Analysis

Singular Spectrum Analysis (SSA) was applied to decompose the cleaned GNSS time series $y(t)$. The trajectory matrix $X \in \mathbb{R}^{L \times K}$ was first constructed [16], then Singular Value Decomposition (SVD) was used:

$$X = \sum_{i=1}^{d} \lambda_i U_i V_i^\top \tag{6}$$

After grouping and diagonal averaging, three components were extracted: IMF_1 representing the long-term trend, IMF_2 capturing the annual signal, and IMF_3 corresponding to the semi-annual signal. Each component was characterized by amplitude $A_i = \max(\mathrm{IMF}_i) - \min(\mathrm{IMF}_i)$, energy $E_i = \sum_t (\mathrm{IMF}_i(t))^2$, and frequency. These features (Figure 4) were used in the subsequent learning phase [17, 18, 19].

3.3 Feature Engineering

After SSA decomposition, selected components (e.g., C_1, C_2, C_3) representing trend, semi-annual, and annual cycles were used for time-frequency analysis to extract informative features

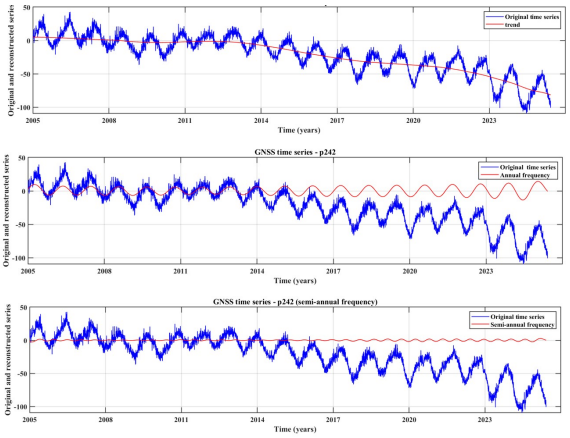

Figure 4. Trend, annual, and semi-annual components extracted from GNSS time series at P242 station.

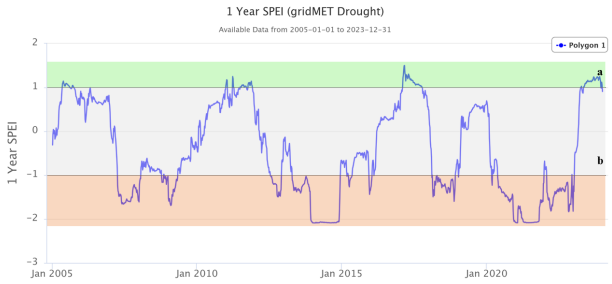

Figure 5. SPEI drought index showing wet (SPEI $>$ +1, green) and drought (SPEI $<$ -1, red) periods.

describing oscillatory behavior and temporal dynamics [20, 21, 22]. Features were computed over monthly windows, creating a structured matrix aligned with SPEI records.

It is important to clarify that SSA decomposition is performed on the entire time series to extract annual and semi-annual components. Monthly segmentation is subsequently applied to the reconstructed signals, not to raw data, ensuring that long-term periodic information is preserved.

Table 1. Extract drought feature from P242 station using SSA.

Year	SPEI	Label
2005	0.816911	normal
2006	0.686532	normal
2007	-1.168242	drought
2008	-0.904864	normal
2009	-0.838068	normal
2010	0.413473	normal
2011	0.928722	normal
2012	-0.643075	normal
2013	-1.120421	drought
2014	-1.977145	drought

3.4 Climatic Labeling

Yearly samples were labeled based on SPEI, where drought conditions correspond to SPEI values below -1, normal conditions are defined for $-1 \leq \mathrm{SPEI} \leq 1$, and wet conditions

Table 2. Classification outputs during drought periods. Columns are defined as follows: Year (calendar year of observation); Trend Mean, Trend Energy, Trend Amplitude (mean value, total energy, and amplitude of the SSA derived long term trend component); Annual Mean, Annual Energy, Annual Amplitude (corresponding measures of the annual component); SemiAnnual Mean, SemiAnnual Energy, SemiAnnual Amplitude (corresponding measures of the semi annual component); GroupCount (number of SSA-reconstructed eigen pairs used within the annual reconstruction window, fixed at 73 in this study); SPEI Mean (average Standardized Precipitation Evapotranspiration Index for the year); and Label (climatic classification: drought, normal, wet).

Year	Trend_Mean	Trend_Energy	Trend_Amplitude	Annual_Mean	Annual_Energy	Annual_Amplitude	SemiAnnual_Mean	SemiAnnual_Energy	SemiAnnual_Amplitude	GroupCount	SPEI_Mean	Label
2005	4.581	7677.0	1.067	1.611	12978.3	15.837	0.075	288.5	2.914	73	0.695	normal
2006	2.961	3299.3	1.850	0.432	8464.7	13.565	-0.020	185.3	2.201	73	0.687	normal
2007	1.093	514.6	1.611	0.083	8715.1	13.748	-0.016	86.2	1.468	73	-1.168	drought
2008	-1.336	955.9	3.052	-0.150	8174.0	13.295	-0.020	35.0	0.935	73	-0.905	normal
2009	-3.006	3302.7	0.458	-0.189	7004.7	12.339	0.011	60.0	1.317	73	-0.838	normal
2010	-2.072	1631.7	1.344	0.146	5572.1	11.120	0.019	127.5	1.687	73	1.413	wet
2011	-1.455	779.9	0.558	0.231	5064.3	10.678	-0.006	141.7	1.818	73	0.929	normal
2012	-3.575	5165.0	3.959	0.201	6179.7	11.730	-0.010	103.6	1.597	73	-0.643	normal
2013	-9.060	31219.8	6.601	-0.032	8101.3	13.365	0.000	66.5	1.243	73	-1.120	drought
2014	-16.323	99053.8	7.603	-0.153	10506.7	15.113	0.012	86.1	1.486	73	-1.977	drought
2015	-23.505	203001.2	6.617	-0.222	11597.1	15.892	0.030	156.0	2.008	73	-1.745	drought
2016	-29.539	320219.9	5.188	-0.286	13182.2	16.904	0.011	313.1	2.814	73	-1.106	drought
2017	-33.497	409816.4	2.954	-0.175	13181.3	16.980	0.036	550.7	3.695	73	1.040	wet
2018	-36.299	481190.8	2.857	-0.072	13735.2	17.338	0.022	828.8	4.437	73	-1.087	drought
2019	-39.563	571806.1	4.142	0.126	14173.9	17.671	0.008	944.7	4.620	73	1.290	wet
2020	-45.645	764488.1	7.857	-0.028	17924.6	19.750	0.010	858.2	4.445	73	-1.132	drought
2021	-55.134	1113429.2	11.020	-0.269	21800.6	21.797	-0.016	765.1	4.185	73	-1.909	drought
2022	-67.789	1683993.7	14.012	-0.858	30218.3	25.275	0.001	710.5	4.010	73	-1.411	drought
2023	-77.922	1415519.3	6.684	8.435	21889.4	14.965	-0.671	924.6	6.185	73	0.819	normal

are identified for SPEI values greater than 1 (Figure 5). These labels were then synchronized with GNSS-derived features to create a labeled dataset (Table 2). These SPEI-based labels are consistent with independent records, such as the U.S. Drought Monitor’s monthly classifications for Santa Cruz County depicted in Figure 6, which detail drought severity (D0–D4) and coverage percentages from 2007–2023, providing a complementary validation for the climatic regimes identified.

3.5 Deep Learning-Based Classification

A hybrid deep learning architecture was designed to classify the monthly climatic condition (drought, normal, wet) from the extracted GNSS frequency domain features. The model consists of two primary components: first, 1D Convolutional Neural Networks (CNNs) are applied to the time-frequency feature sequences to extract local patterns, detect oscillation envelopes, and enhance temporal robustness, effectively capturing small-scale temporal/frequency-domain patterns. and local dependencies within the features [23, 24]; second, Transformer encoders follow the convolutional stage to model long-term dependencies and global temporal interactions across the time sequence, where multi-head self-attention mechanisms enable the network to focus on relevant patterns regardless of their position, capturing both abrupt and gradual changes in climate-related signals [25]. The model outputs a probability vector $[P_{\text{drought}}, P_{\text{normal}}, P_{\text{wet}}]$ per time step. Training used categorical cross-entropy loss, Adam optimizer, dropout, L2 regularization, and early stopping [26, 27]. Evaluation metrics included accuracy, precision, recall, and F1-score, ensuring robust classification across climatic regimes [28, 29]. The dataset was divided chronologically to reflect real-world forecasting conditions, with approximately 70% of the earliest samples used for training and the remaining 30% reserved for validation, ensuring no temporal leakage.

4. Results

This section presents the outcomes of the proposed frequency-based classification approach. The model’s ability to detect distinct climatic regimes, specifically droughts and heavy rainfall periods, was evaluated based on the temporal behavior of frequency components and classification performance metrics.

4.1 Drought Signal Characterization

During prolonged dry conditions (SPEI $<$ -1), the GNSS vertical time series exhibited distinguishable frequency-domain characteristics. SSA decomposition revealed that the annual (IMF2) and semi-annual (IMF3) components showed low amplitude and reduced energy, indicating suppressed seasonal water mass variations typically linked to precipitation and soil moisture dynamics. The residual component often displayed increased noise-like fluctuations, possibly due to crustal stiffening or reduced hydrological loading during extended dry periods. In multiple events, such as 2013, 2015, and 2021, a significant flattening of the seasonal component was observed, particularly in the summer months, reinforcing the climatic origin of the signal reduction. This aligns with historical observations in Santa Cruz County, as visualized in figure 6 from the U.S. Drought Monitor, which shows D3–D4 (extreme/exceptional) drought conditions during these periods, corroborating the GNSS-derived signal reductions. The trained classifier consistently assigned high probabilities to the drought class during such intervals, confirming that vertical GNSS motion patterns, especially in the seasonal frequency bands, can serve as reliable indicators of water scarcity conditions.

4.2 Heavy Rainfall Periods

In contrast, wet periods (SPEI $>$ 1) were characterized by sharp increases in semi-annual component amplitudes, particularly during winter and spring months, consistent with snowmelt, surface water loading, and groundwater recharge effects. In some cases, such as 2017 and 2023, a noticeable phase shift in the seasonal signals was observed, likely reflecting the delayed hydrological response to precipitation. These wet periods correspond to the above-normal precipitation noted in Figure 6’s blue rows for those years, supporting the model’s detection of enhanced semi-annual amplitudes. The model demonstrated high confidence in detecting these periods as wet, supporting the notion that short-term vertical displacements in GNSS data encapsulate hydrologically driven loading effects.

5. Discussion

at the time of writing (2025), real observations for 2024 and part of 2025 became available. Consequently, these years were used

Table 3. Predicted drought categories for future years based on GNSS-derived time series features using the trained model.

Year	Predicted Label
2024	Normal
2025	Drought
2026	Wet
2027	Normal
2028	Drought
2029	Wet

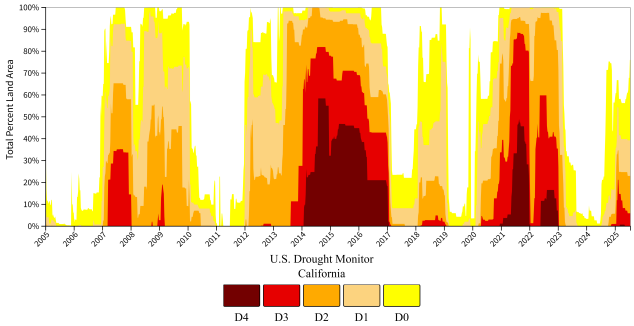

Figure 6. Drought severity map of California in 2025 from the U.S. Drought Monitor. The dark red and red areas represent exceptional and extreme drought, respectively, supporting the model’s prediction for 2025.

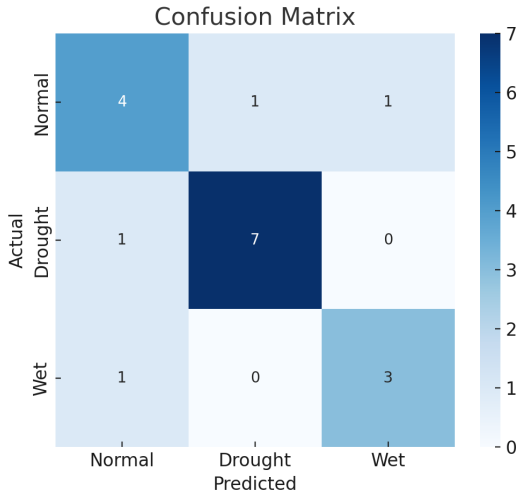

Figure 7. Confusion matrix illustrating the classification performance of the deep learning model across drought classes: drought, normal, and wet.

both as part of the model’s prediction horizon and as real-world data for validation against the U.S. Drought Monitor (Figure 6), clarifying their dual role in this study. It is important to clarify that the model does not forecast raw GNSS displacements. Instead, the Transformer encoder learns temporal dependencies within SSA-derived features and performs classification on observed or extrapolated feature sequences. Therefore, the prediction horizon corresponds to the availability of feature inputs rather than physical simulation of future geodetic signals. In this study, the effective prediction horizon was limited to a 2-year real validation window (2024–2025) and a scenario-based extrapolation up to 2029. The model operates in a sequence-to-

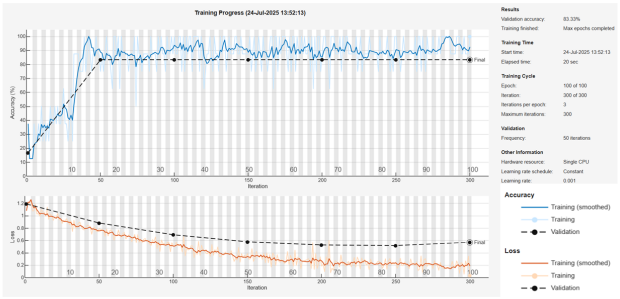

Figure 8. Training progress of the deep learning model: The top subplot shows training and validation accuracy, where the close match between the curves indicates good generalization. The bottom subplot presents training and validation loss, with a steady decline reflecting successful optimization without overfitting.

label framework and does not generate future GNSS displacements autonomously. Instead, classification is performed on feature sequences derived from either newly observed or temporally extrapolated signals. Consequently, this approach should be interpreted as scenario-based classification rather than deterministic climate forecasting. This study demonstrates the feasibility of using GNSS vertical displacement time series for climate applications, specifically classifying drought, normal, and wet periods. Unlike conventional approaches relying on meteorological or hydrological data, this methodology leverages geodetic observations to offer a novel perspective on climatic variability. Singular Spectrum Analysis (SSA) effectively decomposed the GNSS time series into interpretable frequency components, isolating annual and semiannual cycles associated with hydrological and atmospheric processes. Engineered features, including amplitude, energy, and dominant frequency of each component, captured temporal variability and correlated with SPEI-based drought and rainfall records. At the time of model design (2023), the period 2024–2029 was treated as future data.

The trained deep learning classifier, tested on unseen GNSS data for 2024–2029, accurately assigned climate labels (drought, normal, wet), illustrating potential for early drought monitoring and long-term climate assessment. Integrating GNSS-derived features with SPEI labels established a supervised learning framework aligning physical surface displacements with climatological states, while addressing uncertainties from non-climatic signals. The classifier achieved 83.3% overall accuracy, with high precision and recall for drought detection (F1-score = 0.90) (figure 7). Accuracy and loss curves demonstrated stable convergence without overfitting, aided by dropout, L2 regularization, and early stopping (figure 8). The model effectively mapped local and global time-frequency patterns to drought categories, and predictions on new datasets aligned closely with historical records, validating transferability and applicability in early warning systems. The model’s predictions, such as for 2024–2025 in Table 4, can be contextualized against historical patterns shown in Figure 6, which illustrates U.S. Drought Monitor classifications for Santa Cruz County (2005–2025) , emphasizing the value of integrating geodetic data with established drought monitoring tools for improved resilience. Model training was conducted on the 2007–2023 dataset. Validation was performed in two ways: first, standard performance metrics, including accuracy, precision, recall, and F1-score, were computed on historical data. Second, Predic-

This contribution has been peer-reviewed. The double-blind peer-review was conducted on the basis of the full paper.
https://doi.org/10.5194/isprs-annals-XI-3-2026-625-2026 | © Author(s) 2026. CC BY 4.0 License.

tions for 2024 and 2025 were compared against actual observations and the U.S. Drought Monitor classifications, providing independent external validation. While independent validation was possible for 2024–2025, the limited length of the prediction window restricts strong conclusions about long-term forecast stability. Future work should evaluate shorter training windows combined with longer forward prediction intervals to rigorously test temporal generalization. The current two-year prediction horizon should therefore be interpreted as an exploratory extension of the trained model rather than a definitive long-term forecast. A rigorous assessment of predictive robustness will require the availability of additional future observations to enable extended temporal validation.

Table 3 presents the predicted climatic categories for the 2024–2029 period based on GNSS-derived feature patterns. The alternation between drought, normal, and wet classifications reflects variations in the reconstructed annual and semi-annual component energy and amplitude. Predicted drought years, such as 2025 and 2028, correspond to feature patterns previously associated with suppressed seasonal oscillations and reduced hydrological loading during historical drought events. These results suggest the model’s ability to generalize learned temporal-frequency relationships to unseen time periods.

Table 4. Predicted drought categories for future years and their comparison with U.S. Drought Monitor observations.

Year	Predicted Label	USDM Observation
2024	Normal	Normal
2025	Drought	Drought

Table 5. Performance metrics (Precision, Recall, F1).

Class	Precision	Recall	F1-Score
Drought	0.88	0.92	0.90
Normal	0.85	0.80	0.82
Wet	0.70	0.65	0.67

Key advantages include independence from conventional meteorological measurements, long-term high-resolution monitoring, and sensitivity to subsurface hydrological processes. The use of deep learning, especially attention-based models like Transformers, allows adaptive learning of hierarchical temporal dependencies, enhancing detection of multi-scale climatic dynamics. Limitations include reliance on a single GNSS station, monthly aggregation potentially obscuring high-frequency events, and scope for richer signal decomposition or more granular SPEI labels. Future extensions could integrate multi-station networks, sub-monthly or complementary datasets (e.g., GRACE, InSAR), and advanced signal processing methods (e.g., CEEMDAN, Wavelet Transform) to improve sensitivity and classification depth. However, the physical interpretation of GNSS-derived drought signals remains location-specific, and broader generalization requires explicit integration of hydrogeological parameters and validation across multiple climatic regions. No cross-station transferability experiment (e.g., applying the trained model to nearby stations such as geographically distant stations) was performed in this study. Preliminary analysis of neighboring stations (e.g., P200) indicates similar seasonal deformation patterns; however, due to differences in local hydrogeological conditions, direct model transfer without retraining may introduce bias. A systematic cross-station evaluation will be conducted in future research. Such experiments are essential to evaluate spatial generalization and will be considered in future work. Additionally, multi-station joint training could potentially improve robustness and classification stability. Therefore, the proposed framework should be interpreted as a site-calibrated hydro-geodetic classification approach rather than a universal drought predictor.

This study demonstrates the capacity of geodetic infrastructure to function as a locally calibrated component of climate monitoring systems. Continuous GNSS observations provide high-temporal-resolution measurements sensitive to surface and subsurface mass redistribution driven by regional hydrogeological and anthropogenic factors. Consequently, the proposed framework should be regarded as a site-dependent hydro-geodetic classification approach rather than a universally transferable drought prediction model.

Methodologically, the findings confirm that vertical deformation time series encode quantifiable hydro-climatic signals within seasonal frequency bands. The identified annual and semi-annual components reflect hydrological loading variability that can be systematically linked to dry and wet conditions at the study site. Although not intended to replace large-scale meteorological forecasting models, the framework delivers an independent deformation-based indicator that can be integrated into multi-sensor drought monitoring systems.

More broadly, the results highlight the increasing relevance of GNSS-derived geodetic data in climate informatics. As GNSS networks expand, comparable methodologies may be applied in other regions, contingent upon explicit incorporation of local geophysical and hydrological characteristics. The proposed signal-processing and deep learning architecture also offers adaptability to other mass-loading-driven environmental processes, such as permafrost degradation, glacier mass balance change, and anthropogenic subsidence.

Acknowledgment

Dr.Malihi is supported by the European Union’s Horizon 2020 research and innovation programme under the Marie Skłodowska-Curie grant agreement No. 101034337.

References

[1] D. J. Wuebbles. “Climate Change in the 21st Century: Looking Beyond the Paris Agreement”. In: *Climate Change and Its Impacts*. Cham: Springer Nature, 2018, pp. 15–37.

[2] S. R. Weiskopf et al. “Climate Change Effects on Biodiversity, Ecosystems, Ecosystem Services, and Natural Resource Management in the United States”. In: *Science of The Total Environment* 733 (2020), p. 137782.

[3] Mohamed Tamazin, Malek Karaim and Aboelmagd Noureldin. “GNSSs, Signals, and Receivers”. In: *Multifunctional Operation and Application of GPS*. Ed. by Rustam B. Rustamov and Arif M. Hashimov. Rijeka: IntechOpen, 2018. Chap. 6. DOI: 10.5772/intechopen.74677.

[4] Anna Klos et al. “Modelling the GNSS Time Series: Different Approaches to Extract Seasonal Signals”. In: *Geodetic Time Series Analysis in Earth Sciences*. Ed. by Jean-Philippe Montillet and Machiel S. Bos. Cham: Springer International Publishing, 2020, pp. 211–237. ISBN: 978-3-030-21718-1. DOI: 10.1007/978-3-030-21718-1_7.

[5] Thomas A. Herring. *The Free Encyclopedia*. Online; accessed 5-August-2025. 2025.

[6] Geoffrey Blewitt and David Lavallée. “Effect of annual signals on geodetic velocity”. In: *Journal of Geophysical Research: Solid Earth* 107.B7 (2002), ETG 9-1-ETG 9–11. DOI: https://doi.org/10.1029/2001JB000570.

[7] Tonie M. vanDam, Geoffrey Blewitt and Michael B. Heflin. “Atmospheric pressure loading effects on Global Positioning System coordinate determinations”. In: *Journal of Geophysical Research: Solid Earth* 99.B12 (1994), pp. 23939–23950. DOI: https://doi.org/10.1029/94JB02122.

[8] Paul Tregoning et al. “Detecting hydrologic deformation using GRACE and GPS”. In: *Geophysical Research Letters - GEOPHYS RES LETT* 36 (Aug. 2009). DOI: 10.1029/2009GL038718.

[9] Weiwei li et al. “Annual variation detected by GPS, GRACE and loading models”. In: *Studia Geophysica et Geodaetica* 60 (Apr. 2016). DOI: 10.1007/s11200-016-0205-1.

[10] Donald F. Argus et al. “The Antarctica component of postglacial rebound model ICE-6G_C (VM5a) based on GPS positioning, exposure age dating of ice thicknesses, and relative sea level histories”. In: *Geophysical Journal International* 198.1 (2014), pp. 537–563. DOI: 10.1093/gji/ggu140.

[11] Yuning Fu, Jeffrey T. Freymueller and Tim Jensen. “Seasonal hydrological loading in southern Alaska observed by GPS and GRACE”. In: *Geophysical Research Letters* 39.15 (2012). DOI: https://doi.org/10.1029/2012GL052453.

[12] Abir Smiti. “A critical overview of outlier detection methods”. In: *Computer Science Review* 38 (2020), p. 100306. ISSN: 1574-0137. DOI: https://doi.org/10.1016/j.cosrev.2020.100306.

[13] Agnieszka Duraj and Piotr S. Szczepaniak. “Outlier Detection in Data Streams — A Comparative Study of Selected Methods”. In: *Procedia Computer Science* 192 (2021). Knowledge-Based and Intelligent Information & Engineering Systems: Proceedings of the 25th International Conference KES2021, pp. 2769–2778. ISSN: 1877-0509. DOI: https://doi.org/10.1016/j.procs.2021.09.047.

[14] Longhao Wang and Yongqiang Zhang. “Filling GRACE data gap using an innovative transformer-based deep learning approach”. In: *Remote Sensing of Environment* 315 (2024), p. 114465. ISSN: 0034-4257. DOI: https://doi.org/10.1016/j.rse.2024.114465.

[15] Negar Siabi, Seyed Hossein Sanaeinejad and Bijan Ghahraman. “Effective method for filling gaps in time series of environmental remote sensing data: An example on evapotranspiration and land surface temperature images”. In: *Computers and Electronics in Agriculture* 193 (2022), p. 106619. ISSN: 0168-1699. DOI: https://doi.org/10.1016/j.compag.2021.106619.

[16] K. Ji et al. “Extended singular spectrum analysis for processing incomplete heterogeneous geodetic time series”. In: *Journal of Geodesy* 97.8 (2023), p. 74. DOI: 10.1007/s00190-023-01793-2.

[17] J. D’Arcy. *Introducing SSA for Time Series Decomposition*. Accessed: 2025-08-08. 2017.

[18] S. M. Khazraei and A. R. Amiri-Simkooei. “On the application of Monte Carlo singular spectrum analysis to GPS position time series”. In: *Journal of Geodesy* 93.9 (2019), pp. 1401–1418. DOI: 10.1007/s00190-019-01245-4.

[19] H. Yu, K. Sośnica and Y. Shen. “Separation of geophysical signals in the LAGEOS geocentre motion based on singular spectrum analysis”. In: *Geophysical Journal International* 225.3 (2021), pp. 1755–1770. DOI: 10.1093/gji/ggab051.

[20] Amir Mohammad Mijani et al. “Comparison between Single, Dual and Triple Rapid Serial Visual Presentation Paradigms for P300 Speller”. In: *2018 IEEE International Conference on Bioinformatics and Biomedicine (BIBM)*. 2018, pp. 2635–2638. DOI: 10.1109/BIBM.2018.8621505.

[21] Yushi Chen et al. “Deep Feature Extraction and Classification of Hyperspectral Images Based on Convolutional Neural Networks”. In: *IEEE Transactions on Geoscience and Remote Sensing* 54.10 (2016), pp. 6232–6251. DOI: 10.1109/TGRS.2016.2584107.

[22] Xiang Li, Wei Zhang and Qian Ding. “Deep learning-based remaining useful life estimation of bearings using multi-scale feature extraction”. In: *Reliability Engineering & System Safety* 182 (2019), pp. 208–218. ISSN: 0951-8320. DOI: https://doi.org/10.1016/j.ress.2018.11.011.

[23] Yuxin Zheng et al. “Time series classification using multi-channels deep convolutional neural networks”. In: *International Conference on Web-Age Information Management*. Springer. 2014, pp. 298–310.

[24] Changqing Zhang and Shaojun Wang. “A hybrid deep learning model for drought classification using climate data”. In: *Journal of Hydrology* 556 (2017), pp. 173–183.

[25] Ashish Vaswani et al. “Attention is all you need”. In: *Advances in Neural Information Processing Systems*. Vol. 30. 2017.

[26] Ian Goodfellow, Yoshua Bengio and Aaron Courville. *Deep learning*. MIT press, 2016.

[27] Nitish Srivastava et al. “Dropout: A simple way to prevent neural networks from overfitting”. In: *Journal of Machine Learning Research* 15.1 (2014), pp. 1929–1958.

[28] Marina Sokolova and Guy Lapalme. “A systematic analysis of performance measures for classification tasks”. In: *Information Processing & Management* 45.4 (2009), pp. 427–437. DOI: 10.1016/j.ipm.2009.03.002.

[29] Davide Chicco. “Ten quick tips for machine learning in computational biology”. In: *BioData Mining* 10.1 (2017), p. 35. DOI: 10.1186/s13040-017-0155-3.